

Article

An Investigation on the Teeth Crowning Effects on the Transient EHL Performance of Large-Scale Wind Turbine Spur Gears

Hazim U. Jamali ¹, H. S. S. Aljibori ², Muhsin Jaber Jweeg ³, Oday I. Abdullah ^{4,5,6,*}
and Alessandro Ruggiero ^{7,*}

¹ Mechanical Engineering Department, College of Engineering, University of Kerbala, Karbala 56001, Iraq; hazimumran@uokerbala.edu.iq

² Al-Warith Center for Crowd Engineering and Management Research, University of Warith Al-Anbiyaa, Karbala 56001, Iraq; hakim.s@uowa.edu.iq

³ College of Technical Engineering, Al-Farahidi University, Baghdad 00965, Iraq; muhsin.jweeg@uofarahidi.edu.iq

⁴ Department of Energy Engineering, College of Engineering, University of Baghdad, Baghdad 10071, Iraq

⁵ Mechanical Engineering Department, College of Engineering, Gulf University, Sanad 26489, Bahrain

⁶ Department of Mechanics, Al-Farabi Kazakh National University, Almaty 050040, Kazakhstan

⁷ Department of Industrial Engineering, University of Salerno, 84084 Fisciano, Italy

* Correspondence: oday.abdullah@tuhh.de (O.I.A.); ruggiero@unisa.it (A.R.)

Abstract: Crowning is applied to wind turbine gears, including spur gears, to ensure adequate stress distribution and contact localization in wind turbine main gearbox gears to improve the gear performance in the presence of misalignments. Each gear tooth is crowned along the face width using a parabolic curve that graduates from a maximum height at the edges and vanishes at the center of the tooth flank. This crowning transfers the elastohydrodynamic contact problem from a line to a point contact case where the surface curvatures and pressure gradient are considered in both directions of the solution space. A wide range of longitudinal crowning heights is considered in this analysis under heavily loaded teeth for typical large-scale wind turbine gears. Furthermore, the variation in the velocities is considered in the analysis. The full transient elastohydrodynamic point contact solution considers the non-Newtonian oil behavior, where the numerical solution is based on the finite difference method. This work is focused on the evaluation of the effectiveness of teeth's longitudinal crowning in terms of the consequences on the resulting pressure distribution and the corresponding film thickness. The modification of the tooth flank significantly elevates the film thickness levels over the zones close to the tooth edges without a significant increase in the pressure values. Moreover, the zone close to the tooth edges from both sides, where the pressure is expected to drop to the ambient pressure, is extended as a result of the flank modification.

Keywords: crown; spur gear; large scale; wind turbine; transient solution



Citation: Jamali, H.U.; Aljibori, H.S.S.; Jweeg, M.J.; Abdullah, O.I.; Ruggiero, A. An Investigation on the Teeth Crowning Effects on the Transient EHL Performance of Large-Scale Wind Turbine Spur Gears. *Lubricants* **2023**, *11*, 462. <https://doi.org/10.3390/lubricants11110462>

Received: 7 September 2023

Revised: 1 October 2023

Accepted: 27 October 2023

Published: 29 October 2023



Copyright: © 2023 by the authors. Licensee MDPI, Basel, Switzerland. This article is an open access article distributed under the terms and conditions of the Creative Commons Attribution (CC BY) license (<https://creativecommons.org/licenses/by/4.0/>).

1. Introduction

The use of wind energy in the energy supply sector has increased and is expected to increase more in the coming years as the cost of this type of energy supply steadily falls [1]. Recently, the capacity of global wind power has grown at an annual rate of 20%, which, therefore, makes wind energy the most significant source of renewable energy on a global scale [2]. The maintenance of the reliability of the wind turbine components at a high level is one of the most significant aspects in this industry to ensure a fail-safe supply of power [3]. The gearbox represents a central component in wind turbine design, where its cost and reliability are considered critical factors in the overall success of the system design. Historically, the industry of wind turbines has been plagued with the failures of gearboxes. These failures have significantly hampered the production of energy, which also have placed an additional burden of high maintenance on the operators of wind turbines [4]. The

wind turbine harnesses wind as a power source and acts as an energy conversion system to produce electricity. Therefore, the continuous changing in the speed and direction of the wind, in addition to rotor dynamics, results in a very unsteady load on the gearbox. Therefore, these factors are having their impacts on the performance of the gearbox. Spur gears, which are used in wind turbines, have drawn the attention of researchers due to the wide range of problems that arise throughout the meshing cycle, where torque and rotation transmit between the axes. One of these significant problems that affects the safe operation of spur gears is the transmission error, which is essentially a rotation delay between the engaged gears. The main reasons for transmission error are the elastic deformation under heavy load and errors related to the alignment and manufacturing processes. Transmission error results in a serious tooth impact at the change points, which is one of the main sources of gear noise and vibration. Meanwhile, edge contact often takes place as a result of this error, which causes a significant stress concentration at the edges. Edge contacts have severe negative consequences on the gears' life [5]. Operating the gears system under heavy loading conditions with a high level of strength has made the tooth modification and optimization of the gear design important research areas in this field [5]. Many researchers suggested using a modified shape of the gear tooth to improve the general performance and to avoid edge contact [6–8]. The effect of tooth profile modification on the performance of a spur gear was investigated by Hou et al. [9]. Their results showed that modifying the tooth flank plays an important role in improving the lubrication state of the teeth, narrowing the range of fluctuation in the transmission error, and dropping the flash temperature. However, they only used the Dowson–Higginson formula for estimating the minimum film thickness without obtaining the lubricant thickness and the corresponding elastohydrodynamic pressure distribution over the entire contact region.

On the other hand, surface wear is one of the major failure modes in gear systems [10]. This mode of failure alters the gear tooth profile, which reduces the efficiency and accuracy of the gear transmission in addition to its effect on the aggravation of the system's vibration and noise characteristics [11,12]. Misalignment is a major cause of surface wear in spur gear teeth [13]. The problem of misalignment in gear systems has drawn the attention of researchers, and various suggestions are now available in the literature regarding the solution to this problem. Zhang et al. [13] used a quasi-static model to study the misalignment effects on the spur gear wear. They used a crown modification strategy, which decelerated the surface wear effectively, and the results suggested that crown height should be chosen depending on the misalignment level; otherwise, the wear depth will not significantly decrease. However, their use of the quasi-static model ignores the time-varying parameters that significantly affect the behavior of the contact between the gear teeth during the meshing cycle. Kumar et al. [14] showed that parallel and angular gear misalignments decrease the effective area of the contact, which causes an increase in the levels of the contact stresses and accelerates gear surface failure.

Assembly errors cause the misalignment of gear coupling shafts, which has a severe negative effect on the working performance of gears. It results in an uneven distribution of the clearance between meshing teeth of the hub and sleeve. Such distribution leads to an unequal tooth load sharing and cyclic loading, and may result in fatigue failure [15]. Gurumani and Shanmugam [5] showed that spur gears are very sensitive to manufacturing errors and the related misalignment, which may result in edge contact. They explained how the edge contact can be avoided by crowning the gear tooth surface. Tran et al. [16] presented a mathematical model for a longitudinal helical gear crowning. The model dealt with a parallel shaving process based on using an auxiliary crowning mechanism to improve the accuracy of the tooth profile and the crowning process. Peng et al. [17] investigated the effects of misalignment and modification on the tribological behavior of helical gears. Their result showed that the edge contact increased the levels of pressure and temperature, and the double-crowning provided a superior tolerance for misalignments and enhanced the lubrication performance of the system. The problem of misalignment in spur gears was also investigated by Beisekenov et al. [18], where they analyzed the bending

and contact stresses of self-aligning automotive spur gear designs with the consideration of various degrees of misalignment. Galym and Spitas [19] presented a novel design of a misalignment-insensitive spur gear transmission based on a Rzeppa joint. Temirkhan et al. [20] developed a novel model for non-conjugate tooth contact for crowned spur and helical gears with the consideration of misalignments. They used this model to assess the effects of misalignment on the contact pressure, transmission error, and the path of contact. Wang and Zhu [21] proposed a model to obtain the mesh stiffness of helical gears under actual lubrication conditions. Recently, Temirkhan et al. [22] presented a quasi-static model for the three-dimensional geometrical non-conjugate contact problem and implemented this model in the crowned teeth in a spur gear in order to estimate the susceptibility to diverse misalignments of the path of contact, transmission error, and contact pressure. Regarding green tribology, which is a relatively new field of tribology, Anand et al. [23] presented an interesting review on the role of this field in the sustainability of mechanical systems. They explained how minimizing wear has a very close relation with green tribology. Wear is the major source for decreasing the machine element lifetime, which therefore requires replacement/recycling. The replacement (or recycling) of the components results in environmental degradation by way of the emission (and waste) innate to the manufacturing process. Furthermore, the debris resulted from wear also has its contribution in the pollution of the environment [23]. Therefore, any reduction in the wear of spur gears resulting from edge contact will contribute to this principle of green tribology. Crowning the gear teeth will be shown in this work to have a positive impact in this direction. Ciulli [24] also illustrated that all tribology branches have several aspects which are related to sustainability, and these aspects can be gathered in the green tribology discipline. The reduction in energy losses as well as the reduction in material consumption are both involved in reducing CO₂ emissions. Adopting a correct tribological design can reduce the wear and friction losses, which helps in this field [24].

This work presents a full transient elasto-hydrodynamic solution of a modified large-scale spur gear used in wind turbines. A point contact model is used in the analysis in order to account for the variation in the surface curvature along the tooth flank due to the modification strategy. The finite difference method is used in this work with the consideration of the non-Newtonian oil behavior. The analyses consider all the time-varying parameters, such as the variation in the surface curvature, load, and surface velocity throughout the meshing cycle. The longitudinal crowning of spur gear teeth is considered to reduce the possibility of thinning the lubricant thickness close to the tooth edges, which is one of the major sources of surface wear due to the severe operating conditions found in wind turbine applications. The variation in rotational speed is also investigated in order to assess the effectiveness of the tooth flank's longitudinal crowning at different levels of the operating speed.

1.1. Surface Curvature and Velocities

The governing equations of the contact problems in spur gears depend on the geometry of the teeth surfaces, surface velocities, and many other aspects, as will be explained later. Figure 1 is used to illustrate the method of determining the radii of curvature for the teeth surfaces in contact in terms of the contact position ζ . This position is defined as the distance from the pitch point along the line of action, and it is positive in the direction shown in this figure. Once the contact position, $CP(\zeta)$, is identified, the radii of curvature can be determined by the following equations, which can be easily derived using the triangles illustrated in Figure 1.

$$R_{x1} = r_1 \tan \lambda + \zeta \quad (1)$$

$$R_{x2} = r_2 \tan \lambda - \zeta \quad (2)$$

where,

r_1 and r_2 are the radii of the base circles of the two gears.

λ is the pressure angle.

ξ is the distance from the pitch point along the line of action.

R_{x1} and R_{x2} are the radii of curvature of the teeth surfaces at a given contact position.

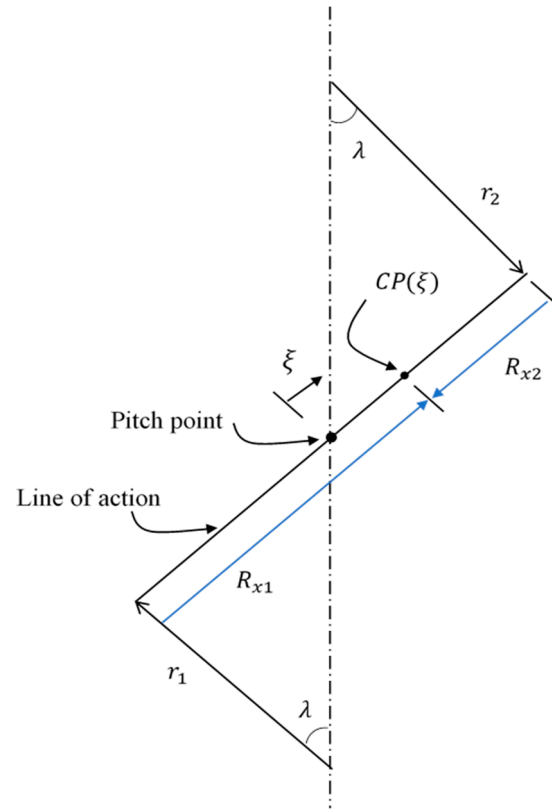


Figure 1. Radii of surface curvature in terms of the distance from the pitch (ξ) along the line of action. $CP(\xi)$ is the contact position along the line of action in terms of ξ .

The equivalent radius of the relative curvature in the tangential direction to the teeth surfaces is

$$\frac{1}{R_x} = \frac{1}{R_{x1}} + \frac{1}{R_{x2}} \quad (3)$$

This radius will be used later (in addition to the curvature due to the flank modification) in determining the undeformed gap between the teeth surfaces. Figure 2 shows the tangent plane of the tooth surfaces at a contact position along the path of contact. The x -axis is normal to the line of action in the illustrated direction, where $x = 0$ at the position shown. The y -axis acts along the face width, and $y = 0$ at the middle of the face width. The normal axis of this plane is the z -axis, which is in the direction of the line of action, and the thickness of the lubricant is identified in this direction. The entrainment speed relative to the contact position is in the x -direction of the x - y plane, which can be determined after calculating the surface speeds relative to the contact position using the following equations.

$$\begin{aligned} u_1 &= (r_1 \tan \lambda + \xi) \Omega_1 \\ u_2 &= (r_2 \tan \lambda - \xi) \Omega_2 \\ \bar{u} &= (u_1 + u_2) / 2 \end{aligned} \quad (4)$$

where,

u_1 and u_2 are velocities of the pinion and the gear teeth surfaces relative to the contact position.

\bar{u} is the entrainment velocity relative to the contact position.

Ω_1 and Ω_2 are the angular speeds of the two gears.

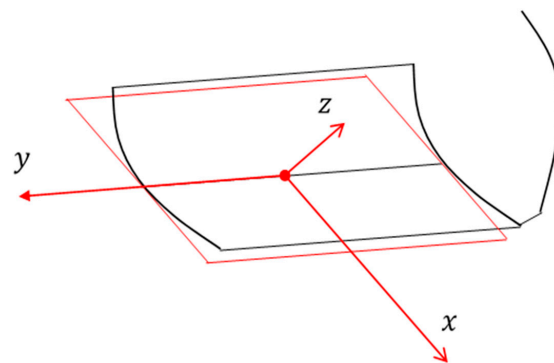


Figure 2. Tangent plane to the teeth surface at a contact position. Single tooth is shown for the purpose of clarity.

1.2. Longitudinal Crowning of the Gear Teeth

The continuous changing of the operating conditions in wind turbines, such as the change in speed and the working under extremely heavy loads, will certainly affect the transient contact in the gear meshing cycle. For example, the angular misalignments between the input and output shafts, which may result from the heavy transmitted load, cause severe negative consequences on the teeth's edges, affecting the system's durability due to the inducing of fatigue spalling [25]. Changing the geometry of the contact, mainly over the edges zone, is illustrated in this section to elevate the level of the lubricant thickness. Such a modification will be examined in detail later to evaluate the effectiveness under heavily loaded conditions of wind turbine spur gears. Figure 3 shows spur gear teeth, and Figure 3a illustrates a typical spur gear with unmodified teeth flanks [26]. In such a case, the resulting contact is a line contact problem. Changing the flank profile using a curved surface, as shown in Figure 3b, transmits the contact problem to a point contact. In contrast to the former case, the point contact problem requires that the surface curvature and the pressure gradient in both directions have to be considered in the solution of the elastohydrodynamic problem of spur gear teeth contact. The solution to the contact problem will be explained in the next section. Regarding Figure 3b, the modification is maximum at the tooth edges and zero at the middle of the tooth flank. Using different values for the crown height (C) will change the resulting gap between the teeth surfaces, which will be examined in the full transient solution of the gear meshing cycle. Figure 4 illustrates the parabolic curve along the face width used in this work when the crown is 50 μm . The maximum value of modification in this figure is 50 μm , which occurs at the edges and gradually decreases to zero at the middle of the face width.

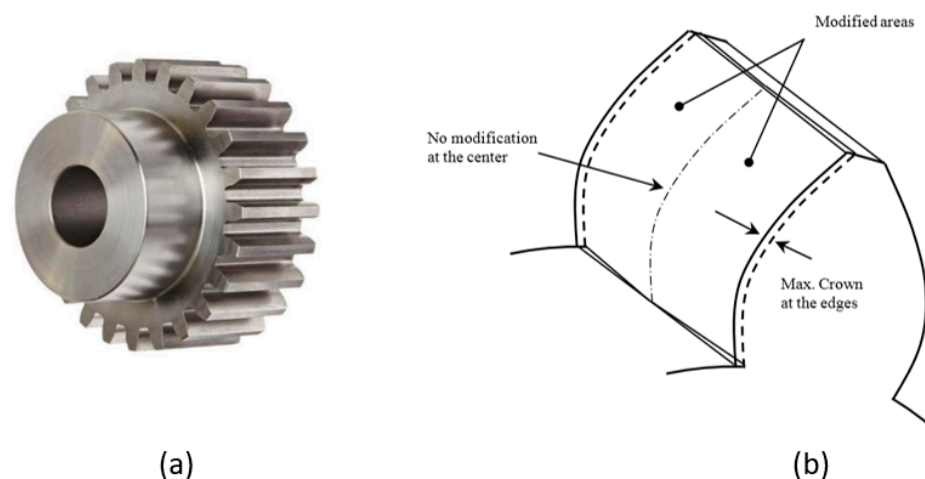


Figure 3. Spur gear teeth. (a) Typical spur gear with unmodified teeth flanks [26] and (b) crowned tooth.

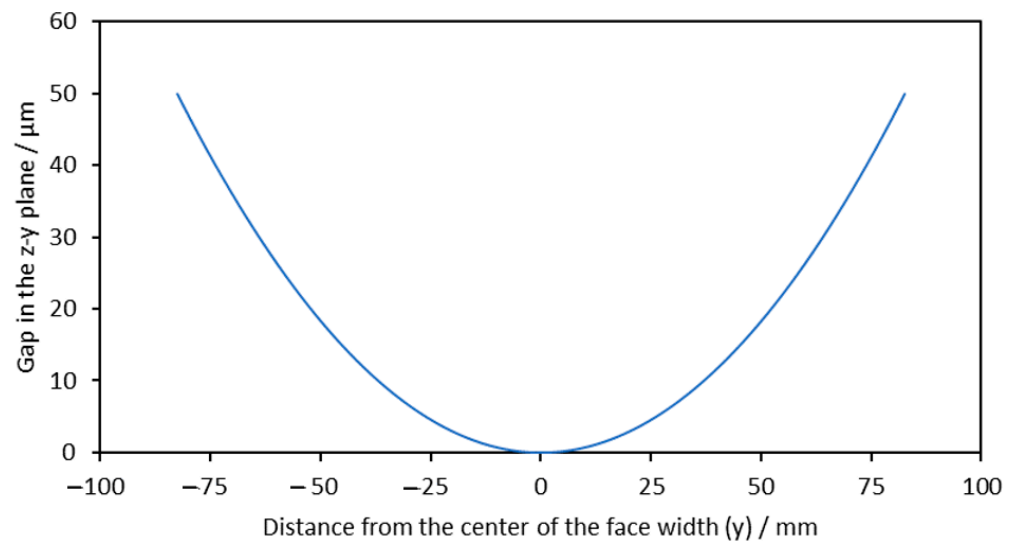


Figure 4. A parabolic curve is used to crown the spur gear teeth in the wind turbine.

2. Governing Equations

The solution of the elastohydrodynamic contact problem in spur gears requires a coupled solution for the two main governing equations, which are the Reynolds and the elastic film thickness equation. If the tooth flank is not modified (there is no curvature in this direction), the one-dimensional Reynolds equation is used in the solution, as the pressure gradient along the face width is ignored, producing a line contact problem. Modifying the tooth flank, as explained previously, produces a curvature along the face width in addition to the curvature along the tooth's involute profile. This means, in other words, that the pressure gradients in both directions of the solution space have to be considered, and a point contact solution is used in this case. The contact problem in spur gears requires a transient solution as the surface curvatures, surface velocities, and load change significantly as the position of contact progresses throughout the meshing cycle. The Reynolds equation for the point contact solution considering the squeeze term (time-dependent term) is given by [27]:

$$\frac{\partial}{\partial x} \left(\kappa_x \frac{\partial p}{\partial x} \right) + \frac{\partial}{\partial y} \left(\kappa_y \frac{\partial p}{\partial y} \right) - \frac{\partial}{\partial x} (\rho \bar{u} h) - \frac{\partial}{\partial y} (\rho \bar{v} h) - \frac{\partial}{\partial t} (\rho h) = 0 \quad (5)$$

The elastic film thickness equation is

$$h(x, y) = \Gamma(x, y) + \Delta(x, y) + \varepsilon \quad (6)$$

where,

ε : Constant.

$\Delta(x, y)$: Teeth surface deformation at a position (x, y) in the solution space.

$\Gamma(x, y)$: The undeformed gap between the teeth surfaces.

x : Axis in the tangential direction to the teeth surfaces.

y : Axis in the direction of the face width of the tooth.

\bar{u} : Mean entrainment velocity, which is given by $\bar{u} = (u_1 + u_2)/2$, where u_1 and u_2 are the surface velocities of the pinion and the gear in the tangential (x) direction, respectively, and $\bar{v} = 0$, as there is no surface velocity in the y direction.

The surface velocities for the pinion and the gear with respect to the contact position were given by Equation (4) previously. In the case of Newtonian oil behavior, the flow factors are given by

$$\kappa_x = \kappa_y = \frac{\rho h^3}{12\eta} \quad (7)$$

In this work, the non-Newtonian oil behavior is considered where the Johnson and Tevaarwerk [28] relation is used. This relation uses the following non-linear form to relate the shear stress and strain rate.

$$\frac{\partial u}{\partial z} = \frac{\tau_0}{\eta} \sinh\left(\frac{\tau}{\tau_0}\right) \quad (8)$$

The viscosity–pressure relation of Roeland [29] in the form suggested by Lugt and Morales [30] is used in this work, which is given by

$$\eta = \eta_0 \exp\left\{ [\ln(\eta_0) + 9.67] \left[\left(1 + \frac{p}{1.962 \times 10^8}\right)^z - 1 \right] \right\} \quad (9)$$

where $z = \frac{1.962 * 10^8 \alpha}{\ln(\eta_0) + 9.67}$.

The Dowson–Higginson [31] equation is used for density–pressure dependency, which is

$$\rho = \rho_0 \left(1 + \frac{\beta p}{1 + \varphi p}\right) \quad (10)$$

The determination of the three terms in the elastic film equation is explained here. In the non-conformal contact problems where the contact between spur gear teeth represents an example of this type of contact, the gap between the surfaces depends on the radii of curvature at each contact position, which was given by Equations (1)–(3) for the tangential direction. Therefore, the total undeformed gap, which is the first term in Equation (6), between the teeth surfaces is given by [32]

$$\Gamma(x, y) = \frac{x^2}{2R_x} + \frac{y^2}{2R_y} \quad (11)$$

where,

R_x (see Equation (3)) and R_y are the equivalent radii of curvature in the x and y directions, respectively.

The equivalent radius of the relative curvature in the y -direction can be calculated using the following equation

$$\frac{1}{R_y} = \frac{1}{R_{y1}} + \frac{1}{R_{y2}} \quad (12)$$

where,

R_{y1} and R_{y2} are the radii of curvature of the teeth surfaces in the y direction. These curvatures result from the longitudinal crowning of the gear teeth, which can be calculated as

$$R_y = \frac{(0.5F)^2}{2C} \quad (13)$$

where,

F is the tooth face width, and C is the crown value at the edges of the tooth.

It is worth mentioning that if the tooth surface is not crowned, the radius of curvature in the y direction becomes infinity (straight line) as C becomes zero in this case. The teeth of the pinion are crowned only as it contains a smaller number of teeth.

The second term in Equation (6), which is the combined surface deformation of the teeth, can be determined by [32]

$$\Delta(\zeta, \vartheta) = \frac{2}{\pi E'} \iint \frac{p(\zeta, \vartheta)}{\sqrt{(x - \zeta)^2 + (y - \vartheta)^2}} dx dy \quad (14)$$

where,

ζ and ϑ are coordinates in the solution space of the point where the deformation is required.

$$\frac{2}{E'} = \frac{1 - \nu_1^2}{E_1} + \frac{1 - \nu_2^2}{E_2}$$

E_1, E_2 : modulus of elasticity of the pinion and the gear materials, respectively.

ν_1, ν_2 : Poisson's ratio of the pinion and the gear materials, respectively.

The third term (ε) in the film thickness equation is determined in the iterative solution, which satisfies the load convergence criterion, as will be illustrated later.

3. Numerical Solution

At each contact position, the radii of curvature, the surface velocities, and the transmitted load are determined as the first step in the solution. The solution space is limited in the y direction by the length of the face width, where the pressure values drop to zero at the boundaries in this direction. On the other side of the solution space (x direction), the boundaries where the pressure values are zero are not exactly known. Therefore, care must be taken before imposing the boundary conditions, as insufficient distance produces incorrect pressure distribution. In this work, an upstream distance of $2.5b$ and a downstream distance of $2b$ (a total distance of $4.5b$) are used as boundaries of the solution space in the tangential x direction, where b is the maximum Hertz dimension in the tangential direction of the resulting ellipse in the case of dry contact. This range ensures the start of pressure generation away from boundaries. It is possible to use a larger distance but at the cost of increasing the number of mesh points, which leads to increasing the required time of the transient solution of the gear meshing cycle.

The governing equations are discretized using the finite difference method using N and M nodes in the x and y directions of the solution space, respectively. The resulting equations are solved using the relaxed alternative direct implicit method. The convergence of the solution is examined based on three criteria. The pressure and film thickness convergence criteria are $\frac{\sum_{j=1}^M \sum_{i=1}^N |p_{(i,j)_{new}} - p_{(i,j)_{old}}|}{\sum_{j=1}^M \sum_{i=1}^N p_{(i,j)_{old}}} < 10^{-5}$ and $\frac{\sum_{j=1}^M \sum_{i=1}^N |h_{(i,j)_{new}} - h_{(i,j)_{old}}|}{\sum_{j=1}^M \sum_{i=1}^N h_{(i,j)_{old}}} < 10^{-5}$, respectively. The load convergence is examined by integrating the resulting pressure field over the entire solution space using the following equation:

$$Load = \iint p(x, y) dx dy = \sum_{j=1}^M \sum_{i=1}^N p(i, j) \Delta x \Delta y \quad (15)$$

The result of this integration is compared with the actual transmitted load, and if it is within a limit of $\pm 1 \times 10^{-4}$ of this load, the convergence of the load is achieved. On the other hand, if this condition is not satisfied, the constant in the film thickness equation (third term) is updated, and the whole solution, which consists of determining the film thickness and the pressure distribution, is repeated until the three convergence criteria are satisfied. This solution procedure is repeated at each contact position along the line of action in order to obtain the full transient solution of the gear meshing cycle. Figure 5 shows a flowchart of the steps used in determining the transient solution of the gear meshing cycle. Different spur gear specifications are used in wind turbine gearboxes [33]. The specifications of the gears used in the current work are explained in Table 1.

Table 1. Gears specifications.

Parameters	Wheel	Pinion
No. of teeth	86	23
Face width	165 mm	
Pressure angle	20 degree	

Table 1. Cont.

Parameters	Wheel	Pinion
Module	7	
Center distance	381.5 mm	
Pitch diameter	602 mm	161 mm
Rotational speed	482 rpm	1800 rpm
Maximum load	109.868 kN	
Load at the first and last contact positions	1/3 Max load	
Load at the end and at the beginning of two pairs in contact periods	2/3 Max. load	

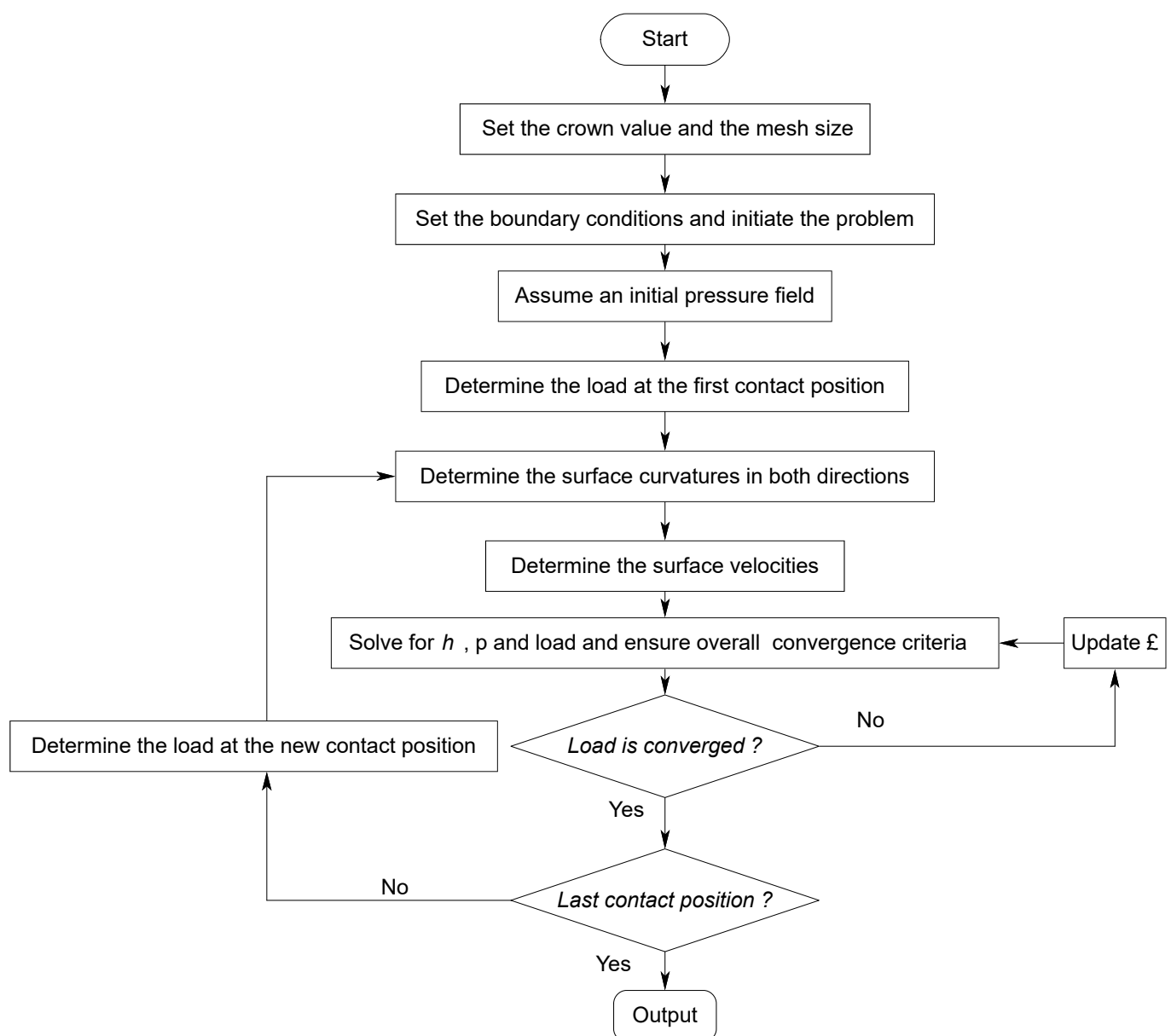


Figure 5. Main solution steps.

4. Results and Discussion

The determination of the undeformed gap between the gear teeth at each contact position depends on the radii of the curvature of the two surfaces. Figure 6 illustrates the variations of the two curvature radii and the resulting radius of relative curvature along the line of action. The difference is very high between the two radii of curvature, R_{x1} and R_{x2} , which is attributed to the difference between the size of the two gears, as explained in Table 1. These values are used in the transient analysis of the teeth meshing cycle. Figure 7 shows the variation in speeds of the surfaces relative to the position of contact along the path of contact in the tangential plane. The mean entrainment speed is also shown in this figure. It can be seen that the difference between the speeds of the surfaces is increased as the position of contact progresses away from the pitch point. The two speeds are equal at the pitch point. Therefore, the mean entrainment speed is equal to the surface speeds at this contact position.

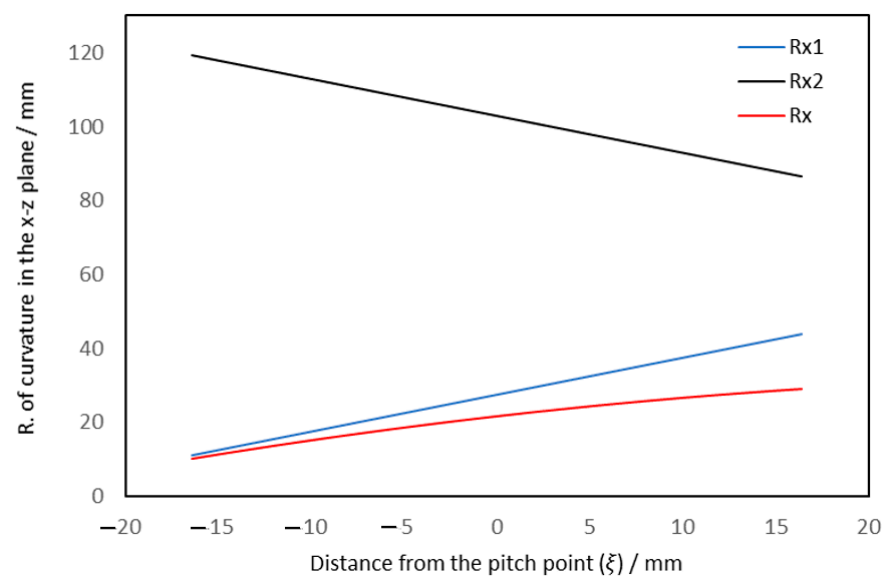


Figure 6. Variation in the curvatures of the teeth surfaces.

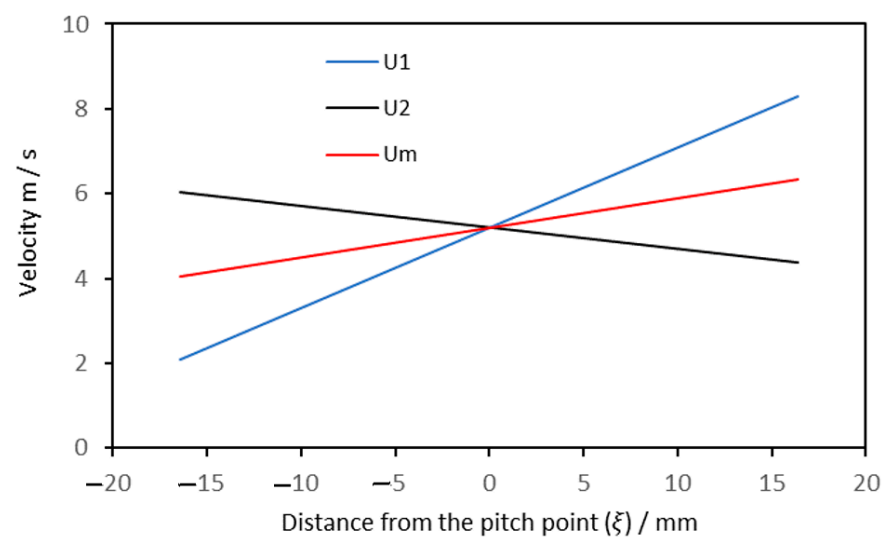


Figure 7. Variation in the surface and entrainment speeds along the path of contact.

Figure 8 shows the variation in p_{max} and h_{min} throughout the full meshing cycle of a pair of teeth in contact. The results shown in this figure are obtained for the case when the value of the maximum modification (crown) is $50 \mu\text{m}$ at the tooth edges. The maximum

pressure (in black) values vary from 1.472 GPa at the first contact to 0.853 GPa at the last contact point. This variation is a result of the transient effects where the radius of curvature, surface velocities of both teeth, as well as the transmitted load are all changed at each contact point. There are sudden changes in the maximum pressure values when $-4.23 \text{ mm} < \xi < 1.71 \text{ mm}$. This distance along the line of action (or, in other words, the period of time from the meshing cycle) corresponds to the situation where there is only a single pair of teeth in contact. In such case, the load is at its highest value, resulting in these sudden changes in the pressure curve. The first change where the pressure rises is due to the start period of this single pair of contact, and the last change where the pressure drops illustrates the starting of the engagement of the second pair of teeth, which shares part of the maximum load. The participation in load sharing causes this drop in the maximum pressure value at this point. Furthermore, at this period of time, the contact continues to face the consequences of this transition to the single pair of contacts where the maximum pressure values fluctuate, as shown in Figure 8. The corresponding minimum film thickness at each contact position is also shown in this figure (in red). The minimum film thickness variation reflects these transient effects and varies from $0.4426 \mu\text{m}$ at the first contact point to $1.044 \mu\text{m}$ at the last contact point.

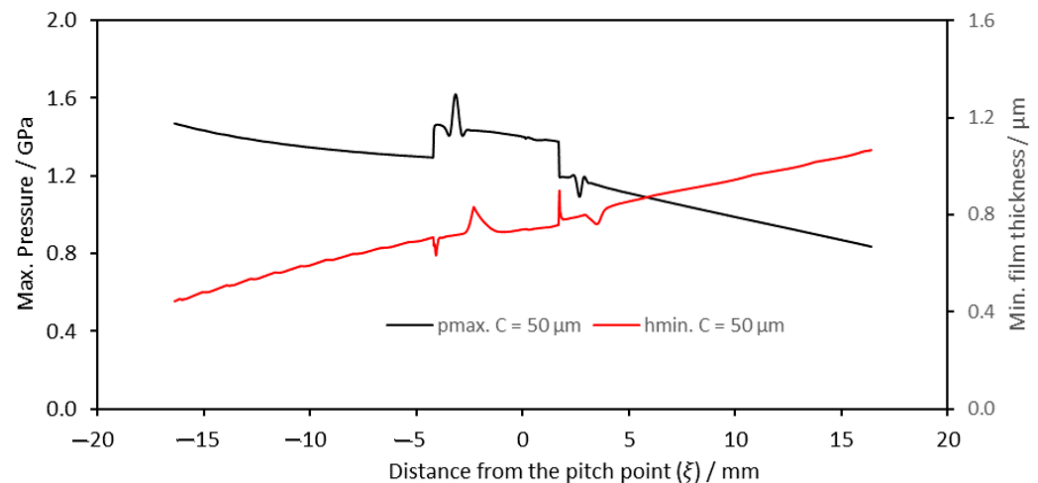


Figure 8. Variation in maximum pressure and minimum film thickness over the teeth meshing cycle when $C = 50 \mu\text{m}$.

Figure 9 shows the pressure distributions at different positions throughout the meshing cycle when the crown is $50 \mu\text{m}$. Nine positions are selected to explain the variation in the pressure contours due to the transient effects. Figure 9a illustrates the contours over three positions in the first period of a double pair of teeth in contact, Figure 9b shows another three contours at the period of the contact between a single pair of teeth, and Figure 9c illustrates a further three contours of the pressure distribution over the second period of a double pair of teeth in contact. It can be seen that in addition to the change in the maximum pressure values through the meshing cycle that is shown in the previous figure, the area of the pressure contour is significantly affected by the position in the meshing cycle. The areas of the contours in the first and second period of a double pair of teeth in contact, as shown in Figure 9a,c, are relatively small in comparison with the contours of the period of the contact between a single pair of teeth, as shown in Figure 9b. The pressure distribution becomes closer to the tooth edges, where $y = \pm 82.5 \text{ mm}$ for the contact in all three contact positions shown in Figure 9b (single pair of teeth in contact). In other words, changing the crown value may result in more aggressive behavior in terms of edge contact, particularly in the severe operating conditions found in wind turbines. Therefore, the effect of crown value on the pressure distribution requires more investigation to ensure safe operation under a wide range of operating conditions. This outcome will be further investigated later in terms of the distance from the tooth edges where the pressure values are zero,

which represents evidence for preventing edge contact. Figure 10 shows the corresponding film thickness contours at these nine positions, where a horseshoe can be seen in all these figures, as is typical for an elastohydrodynamic lubrication regime. It can be seen that crowning the gear teeth elevates the film thickness values close to the tooth edges, which reduces the possibility of edge contact.

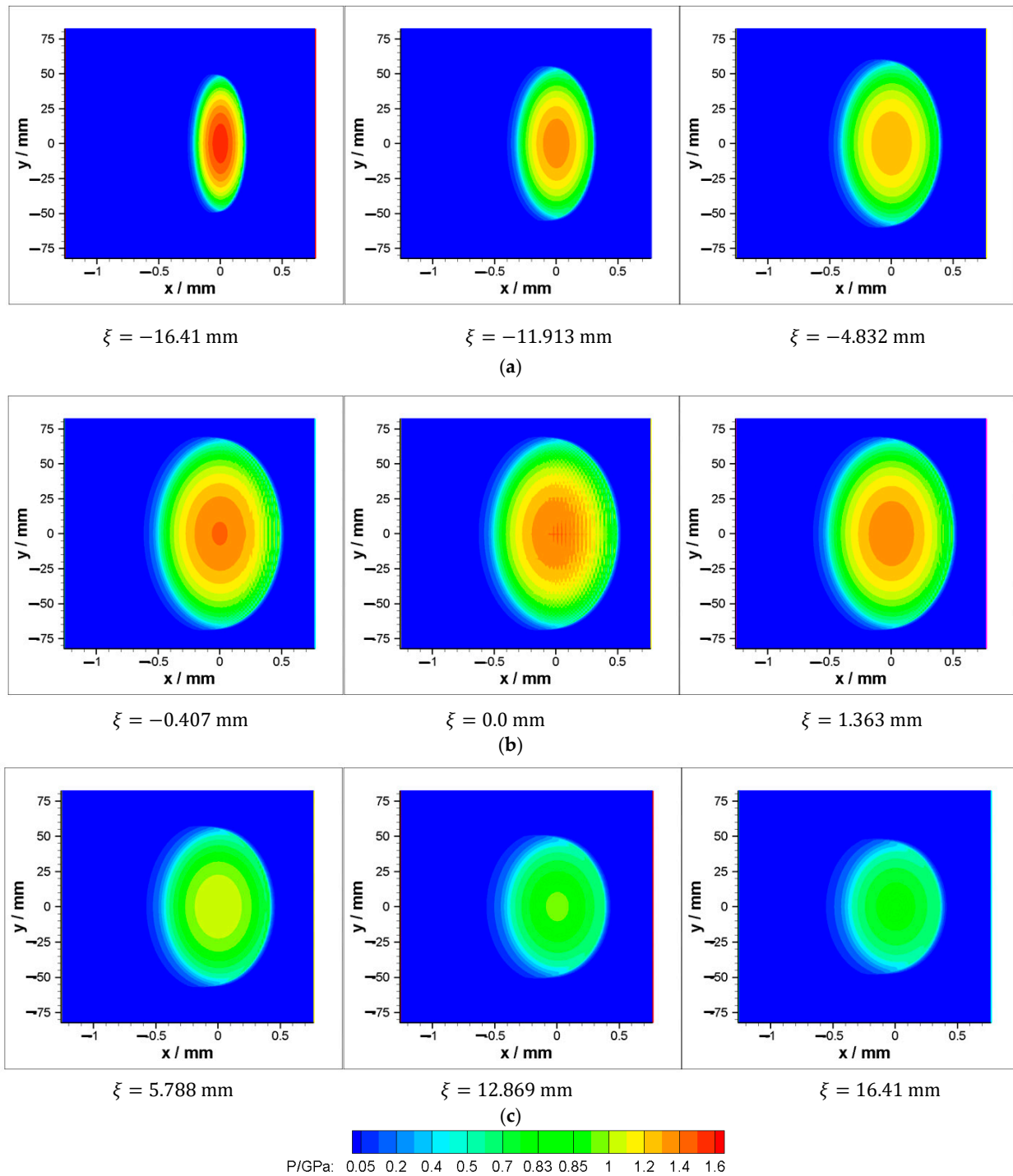


Figure 9. Pressure distribution at different positions throughout the meshing cycle when $C = 50 \mu\text{m}$. (a) First period of double pair of teeth in contact, (b) period of the contact between a single pair of teeth, and (c) second period of double pair of teeth in contact.

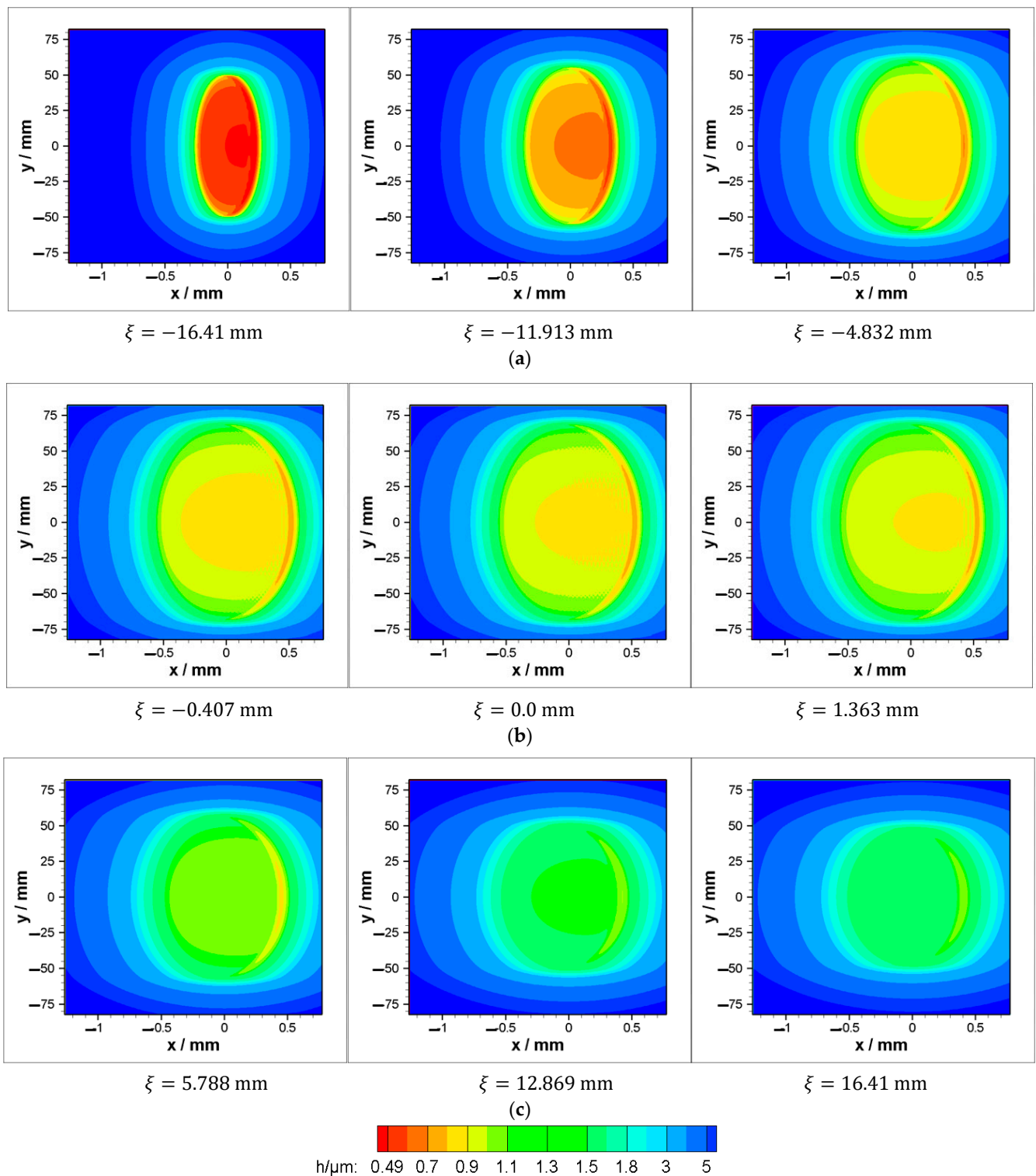


Figure 10. Film thickness contours at different positions throughout the meshing cycle when $C = 50 \mu\text{m}$. (a) First period of double pair of teeth in contact, (b) period of the contact between a single pair of teeth, and (c) second period of double pair of teeth in contact.

The value of crown (C) was $50 \mu\text{m}$ for the results presented in the previous figures, as mentioned previously. The effects of crown value on the transient results are shown in Figure 11. Several values are used, which are less than and greater than $50 \mu\text{m}$. These values are 40, 50, 60, and $100 \mu\text{m}$. It can be seen that increasing the crown value leads to an increase in the maximum pressure and reduces the film thickness in all cases. The

maximum pressure values are 1.503, 1.567, 1.621, and 1.782 GPa when $C = 40, 50, 60,$ and $100 \mu\text{m}$, respectively. However, these increases will be shown later to have fewer drawbacks in comparison with the benefit of the relatively higher values of C in terms of the teeth edge contact. Mathematically, these are expected results, as increasing the crown height at the tooth edges reduces the area over which the pressure is generated for the same transmitted load. In such cases, the pressure values rise over this reduced area in order to have their integration results in the same transmitted load. The corresponding minimum film thicknesses for these crown heights are $0.4538, 0.4426, 0.4326,$ and $0.3885 \mu\text{m}$, respectively. It can be seen that in all cases, the minimum film thickness values are higher than $0.3 \mu\text{m}$, which is considered to be a relatively high level of lubricant layer in the authors' experience in this field, as the gearbox usually operates in a much lower level of film thickness due to the well-known reasons.

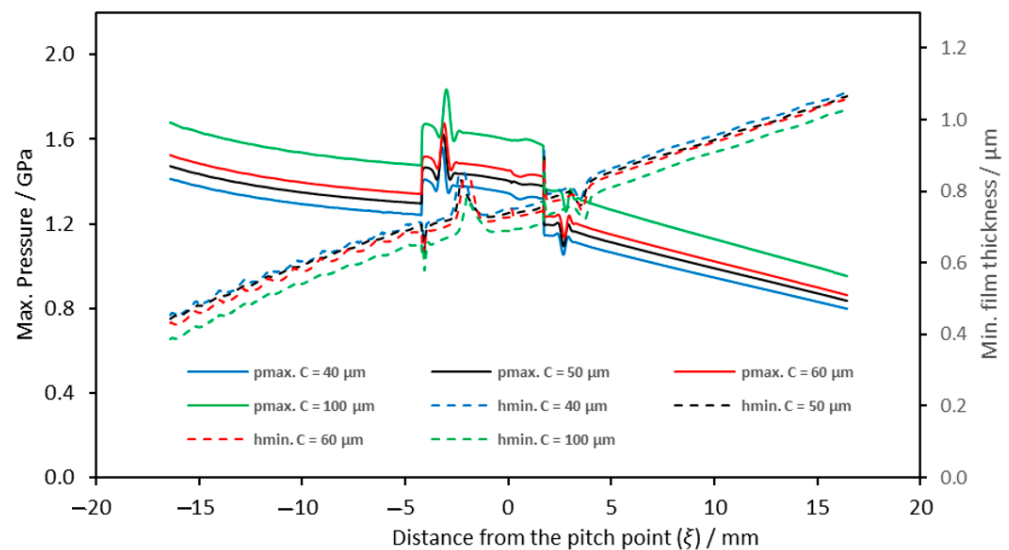


Figure 11. Effect of longitudinal crown value on the maximum pressure and minimum film thickness over the gear meshing cycle.

The transient results presented in the previous figure (Figure 11) do not explain the extent to which the pressure is generated close to the edge of the teeth surfaces. Therefore, Figures 12–14 explain side views (in the y - z plane) for the pressure distributions to illustrate this concept for the whole considered range of longitudinal crowns. Figure 13 shows the pressure distribution of a single pair of teeth in contact at the first period. As the load at this period of the contract is about one-third of the maximum transmitted load, it can be seen that the pressure is generated far from the edges ($y = \pm F/2$) in all cases shown in this figure where different values of the crown are used. However, as the crown value increases, the pressure is generated over the area farthest from the edge. This is very clear when comparing Figure 12a,b, where the crown values are 40 and $100 \mu\text{m}$, respectively. When the crown value is $100 \mu\text{m}$, the distance of zero pressure along the y -axis from both sides is about double the corresponding distance of the case when $C = 40 \mu\text{m}$, and the pressure is increased by only 18.58% (1.503 to 1.7823 GPa). It is worth mentioning that the resulting maximum pressure value is still, despite this increase, less than the pressure value if the film thickness is either dropped to the surface features or if there is any error related to the manufacturing or misalignment. However, when the crown is $60 \mu\text{m}$, the distance of zero pressure is also greater (about 1.4) than the corresponding distance of the case when $C = 40 \mu\text{m}$, and the maximum pressure is only increased by 7.8% (1.503 to 1.6208). Similar behavior is also obtained for the case of $C = 50 \mu\text{m}$, where the distance of zero pressure increases (less increase in comparison to the case of $C = 60$ and $100 \mu\text{m}$) and the pressure slightly increases.

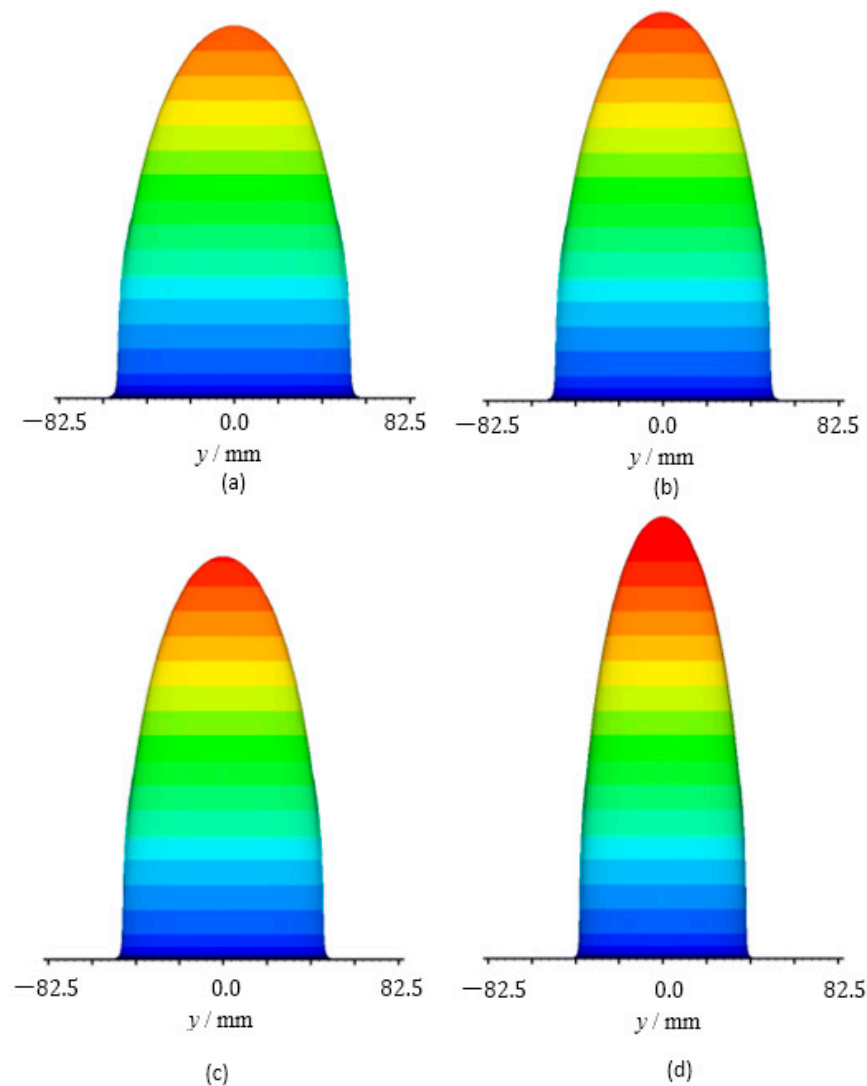


Figure 12. Effect of crown value on the pressure distribution at the first period of double pair of teeth in contact. (a) $C = 40 \mu\text{m}$, (b) $C = 50 \mu\text{m}$, (c) $C = 60 \mu\text{m}$, and (d) $C = 100 \mu\text{m}$.

Figure 13 shows the corresponding results at the period of a single pair of contacts. As explained previously, the transmitted load at this period is at its maximum value. This load level (in addition to the other contact characteristics) affects the area over which the pressure is generated. Figure 13a illustrates the pressure distribution when the crown height is $40 \mu\text{m}$. It can be seen that two pressure spikes are generated very close to the teeth edges (close to $y = \pm F/2$). This figure required an explanation in terms of the imposed boundary condition before solving the governing equations in their discrete forms numerically. The pressure values are set to zero at the boundaries of the solution space. Regarding this figure, the boundary condition at this side of the solution space is zero at $y = \pm F/2$. The results in this figure illustrate that the pressure is generated just next to the boundary nodes. This means, in other words, that the pressure requires a larger distance to be generated over, but it faces zero values at the next node, which is imposed as a boundary condition. In this case, imposing the boundary conditions does not necessarily reflect the actual behavior at the edge of the teeth. Furthermore, a severe thinning of the film thickness, associated with an increase in the pressure value at the edges, is the expected result, which may lead to edge contact or at least increase the wear rate at the teeth edges. The results of this figure illustrate that the value of $C = 40 \mu\text{m}$ is not sufficient to maintain the generation of the pressure away from the teeth's edges. All the other values of the crown height, $C = 50, 60,$ and $100 \mu\text{m}$, clearly help in generating the pressure at a distance far from the teeth edges,

as shown in Figure 13b–d, respectively. The last case, where $C = 100 \mu\text{m}$, gives the best distance, and the pressure is only increased by 16.4% (1.40 to 1.63 GPa) in comparison with the case of $C = 40 \mu\text{m}$ at this position in the meshing cycle.

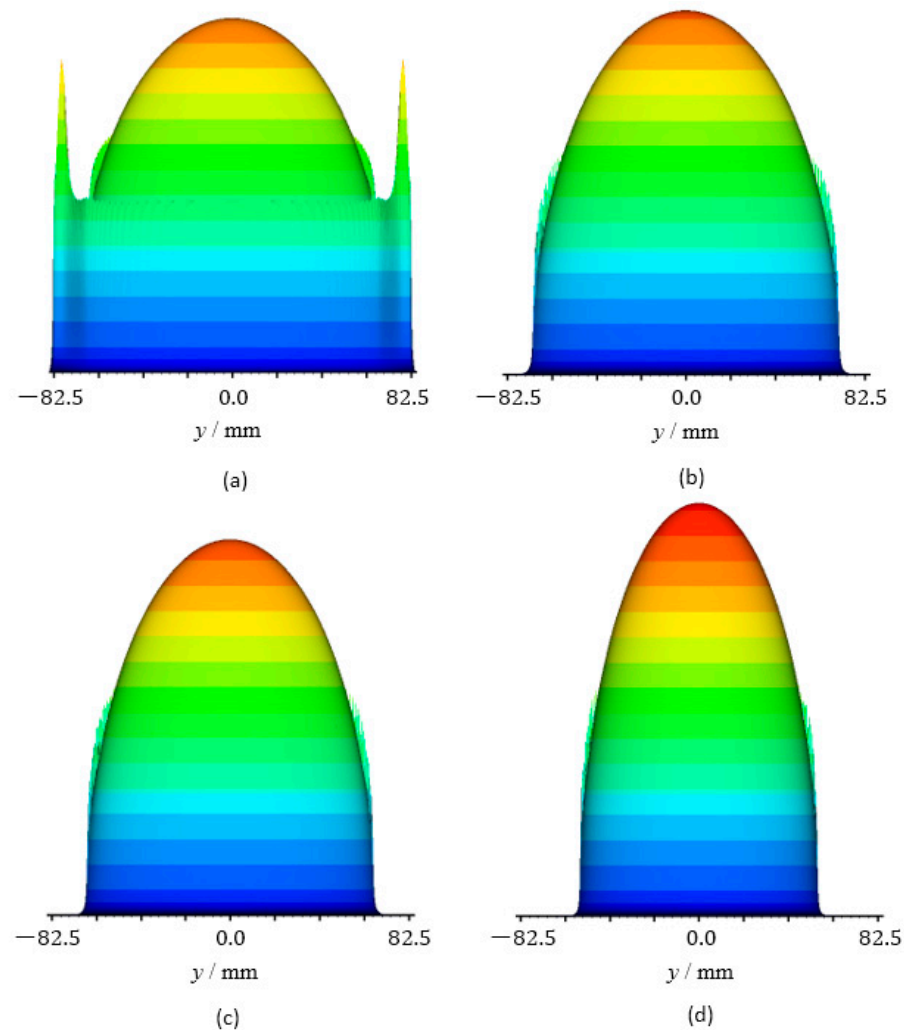


Figure 13. Effect of crown value on the pressure distribution at the period of single pair of teeth in contact. (a) $C = 40 \mu\text{m}$, (b) $C = 50 \mu\text{m}$, (c) $C = 60 \mu\text{m}$, and (d) $C = 100 \mu\text{m}$.

The pressure distributions at the second period of a double pair of teeth in contact for different pressure crown values are shown in Figure 14. In general, there is similar behavior to the results of the first period of a double pair in contact that were shown previously in Figure 12. All the considered crown heights are sufficient enough to maintain a generation of pressure away from the teeth edges, and the maximum pressure slightly increases as the crown height increases.

Figure 15 shows a further comparison between the film thickness as well as the pressure distributions at the center of the face width ($y = 0.0$) when the crown height is 50, 60, and 100 μm . All the distributions are typical elastohydrodynamic results. It can be seen that the pressure distribution when $C = 100 \mu\text{m}$ is wider than the corresponding distribution when $C = 50$ and 60 μm . This is due to the fact that as the length of the area in which the pressure is generated over becomes shorter in the y direction due to the relatively high crown value, the area is extended in the x direction, which is shown in this figure to compensate for a part of this reduction. The other compensation part is clearly in the level of the pressure, which is again clearly higher in this figure than the corresponding pressure levels when $C = 50$ and 60 μm . On the other hand, the film thickness when $C = 100 \mu\text{m}$ is slightly less than the corresponding film thickness levels when $C = 50$ and 60 μm . It is also

clear that the film thickness is flat over longer distances when $C = 100 \mu\text{m}$ for the same previously mentioned reasons.

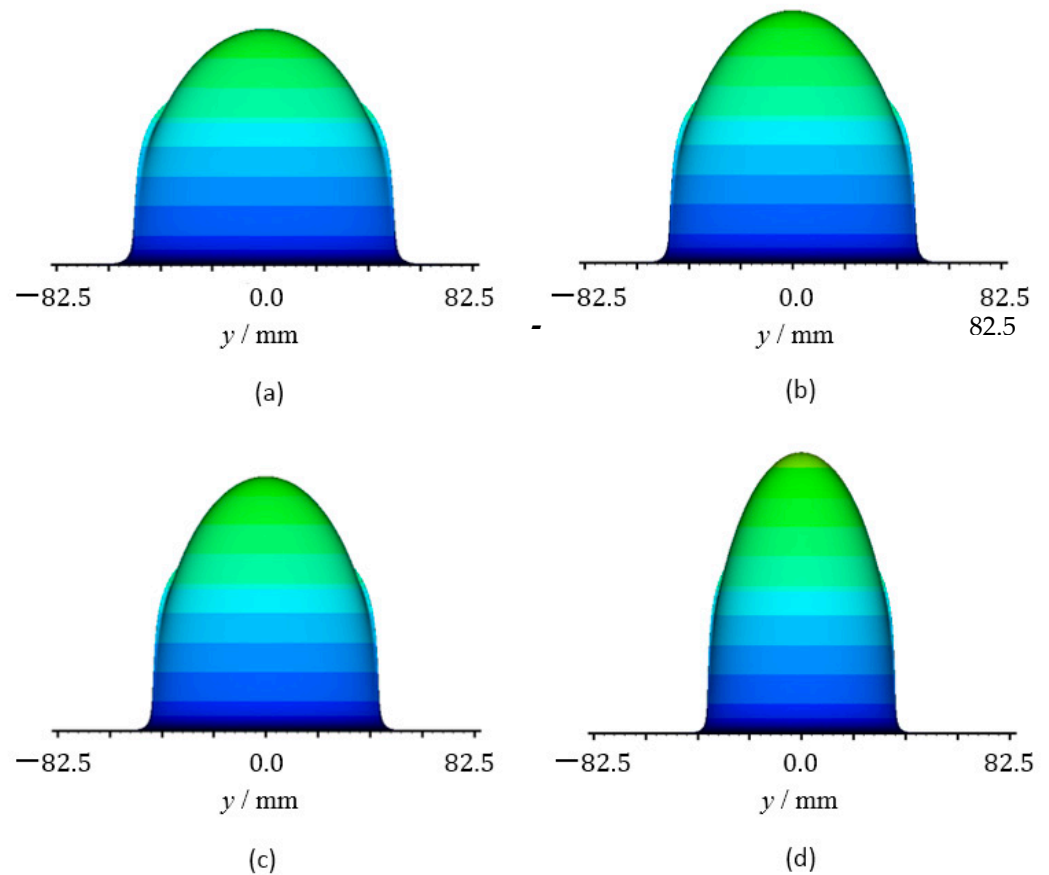


Figure 14. Effect of crown value on the pressure distribution at the second period of double pair of teeth in contact. (a) $C = 40 \mu\text{m}$, (b) $C = 50 \mu\text{m}$, (c) $C = 60 \mu\text{m}$, and (d) $C = 100 \mu\text{m}$.

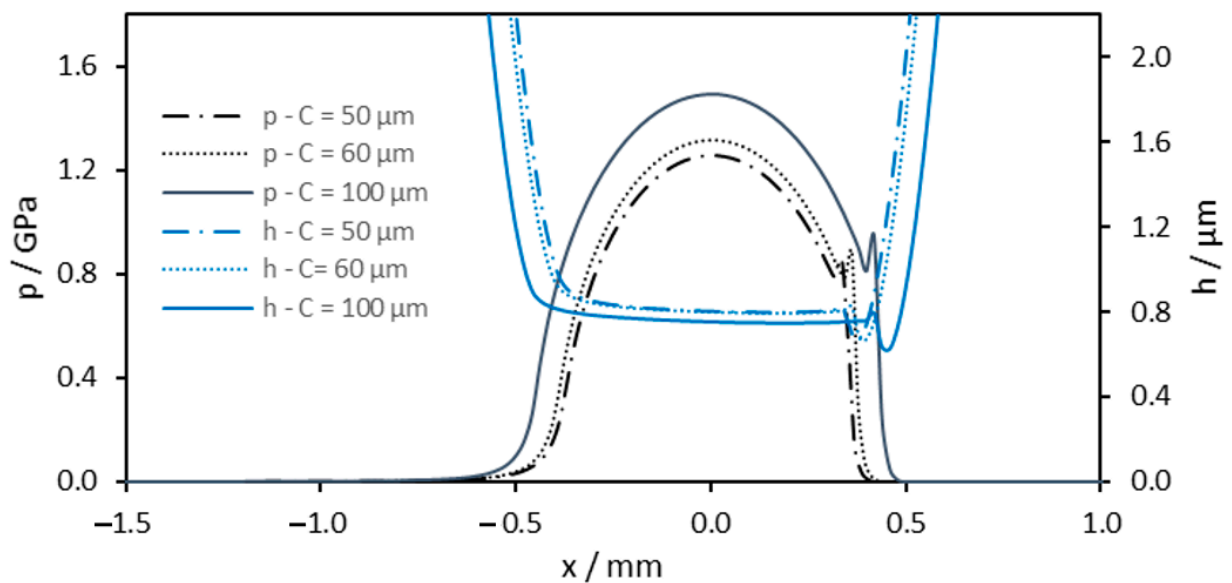


Figure 15. Pressure and film thickness variations at the center of the face width ($y = 0.0$) for different values of the crown height.

The previous figures illustrate that when the crown height is $\geq 50 \mu\text{m}$, the pressure is generated away from the teeth's edges. This distribution helps in reducing the possibility of the thinning of the film thickness at the edges, which may cause an edge contact. Further investigation is performed for the effect of gear rotational speed on the elastohydrodynamic results when the distance is $50 \mu\text{m}$. Tables 2–4 explain these results when the pinion rotational speed is 0.5Ω , Ω , and 1.5Ω , respectively, where Ω is the designed rotational speed used in obtaining all the previous results. Table 2 shows the maximum pressure and minimum film thickness values at the first period of a single pair of teeth in contact when $\zeta = -16.41 \text{ mm}$. It can be seen that as the rotational speed is reduced to 0.5Ω , the minimum film thickness value decreases by 49.66% (from 0.4426 to $0.2228 \mu\text{m}$), and increasing the rotational speed to 1.5Ω increases the minimum film thickness by 37.16% (from 0.4397 to $0.6031 \mu\text{m}$). In all cases, the level of the film thickness is greater than $0.22 \mu\text{m}$, which represents an additional benefit for the longitudinal crowing of the spur gear teeth, as it continuously separates the teeth surfaces by a sufficient layer of the lubricant despite the large change in the speed. The maximum pressure values are less affected by changing the rotational speed. Similar behaviors are also obtained at the position of a single pair of teeth in contact ($\zeta = -1.256 \text{ mm}$) shown in Table 3 and at the position of $\zeta = +2.283 \text{ mm}$ (Table 4), which represents a position in the second period of a double pair of teeth in contact.

Table 2. Effect of rotational speed on p_{max} and h_{min} at the first period of double pairs of teeth in contact ($\zeta = -16.41 \text{ mm}$); $C = 50 \mu\text{m}$.

Pinion Speed	p_{max}	h_{min}	% Diff. in h_{min} (with Respect to the Case of Ω)
Ω	1.472	0.4426	-
0.5Ω	1.477	0.2228	-49.66
1.5Ω	1.467	0.6107	37.98

Table 3. Effect of rotational speed on p_{max} and h_{min} at the period of a single pair of teeth in contact ($\zeta = -1.256 \text{ mm}$); $C = 50 \mu\text{m}$.

Pinion Speed	p_{max}	h_{min}	% Diff. in h_{min} (with Respect to the Case of Ω)
Ω	1.4252	0.7321	-
0.5Ω	1.4173	0.4234	-42.17
1.5Ω	1.4255	0.9760	33.32

Table 4. Effect of rotational speed on p_{max} and h_{min} at the first period of double pairs of teeth in contact ($\zeta = +2.280 \text{ mm}$); $C = 50 \mu\text{m}$.

Pinion Speed	p_{max}	h_{min}	% Diff. in h_{min} (with Respect to the Case of Ω)
Ω	1199.1	0.7867	-
0.5Ω	1191.2	0.4511	-42.66
1.5Ω	1121.6	1.0666	35.58

This work is focused on studying the variation in the tooth profile along the face width. Further investigation is required to incorporate the misalignment effect, the geometry change due to tip relief, and the surface features (roughness). Such a comprehensive model will represent a significant foundation to studying the fatigue failure of the spur gears in the considered large scale used in wind turbines. However, these important issues will be

considered in the near future work. Furthermore, detailed comparisons are also required between the results presented in this work and the results of the misaligned case where the thinning in the lubricant is expected to be very clear at the edges of the teeth, which is also planned to be conducted in future work.

5. Conclusions and Remarks

This work presents a full transient elastohydrodynamic solution of the large-scale spur gear meshing cycle used in wind turbines. The modification of the tooth flank is considered to reduce the negative effects of the severe operating conditions that face the operation of the spur gears in wind turbines, such as the variation in speeds and working under extremely heavy transmitted loads. A parabolic curve is used to modify the tooth flank with a maximum height at the tooth edges and gradually decrease to a value of zero at the middle of the face width. The numerical solution is performed using the finite difference method with the consideration of the non-Newtonian behavior of the lubricant. It has been found that in such large-sized gears and heavily loaded conditions, the value of the crown height needs to be examined carefully, as a few tens of microns may not be sufficient enough to prevent the generation of pressure close to the tooth edges. For a heavy maximum load of 665.9 kN/m (109.9 kN) in the gear meshing cycle, a crown value at the edges of $C \geq 50 \mu\text{m}$ is found to be very effective in generating the pressure away, in considerable distance, from the tooth edges. Furthermore, the film thickness at the tooth edges is also increased due to this modification, which can compensate for any possible reduction in the gap between the surfaces due to misalignment under a heavy transmitted load. The modification is also found to be efficient under the variation in operating speed. These results represent a significant improvement in the performance of the wind turbine gears in terms of the green tribology principles. Further work is required to consider the effect of surface features, misalignment, and the geometry change due to tip relief under the modification of the tooth flank of this size of spur gears. A fatigue analysis is also required in order to assess the impact of the current modification on the lifetime of spur gears.

Author Contributions: Methodology, Investigation, Writing—Review and Editing—Funding Acquisition, Resources, H.U.J. and H.S.S.A.; Validation, Funding Acquisition, Resources, M.J.J.; Formal Analysis, Funding Acquisition, Resources, O.I.A.; Conceptualization and supervision, A.R. All authors have read and agreed to the published version of the manuscript.

Funding: This research received no external funding.

Institutional Review Board Statement: Not applicable.

Informed Consent Statement: Not applicable.

Data Availability Statement: The study did not report any data.

Conflicts of Interest: The authors declare no conflict of interest.

References

1. Rohrig, K.; Berkhout, V.; Callies, D.; Durstewitz, M.; Faulstich, S.; Hahn, B.; Jung, M.; Pauscher, L.; Seibel, A.; Shan, M.; et al. 2019 Powering the 21st century by wind energy—Options, facts, figures. *Appl. Phys. Rev.* **2019**, *6*, 031303. [[CrossRef](#)]
2. Junior, V.J.; Zhou, J.; Roshanmanesh, S.; Hayati, F.; Hajiabady, S.; Li, X.Y.; Dong, H.; Papaalias, M. Evaluation of damage mechanics of industrial wind turbine gearboxes. *Insight-Non-Destr. Test. Cond. Monit.* **2017**, *59*, 410–414. [[CrossRef](#)]
3. Röder, J.; Jacobs, G.; Duda, T.; Bosse, D. Simulative investigation of the load propagation in a wind turbine drive train during a power converter fault. *J. Phys. Conf. Ser.* **2020**, *1618*, 032028. [[CrossRef](#)]
4. Errichello, R.; Muller, J. *Application Requirements for Wind Turbine Gearboxes*; NREL/TP-442-7076; National Renewable Energy Lab: Golden, CO, USA, 1994.
5. Gurumani, R.; Shanmugam, S. Modeling and contact analysis of crowned spur gear teeth. *Eng. Mech.* **2011**, *18*, 65–78.
6. Seol, I.; Kim, D.H. The kinematic and dynamic analysis of crowned spur gear drive. *Comput. Methods Appl. Mech. Eng.* **1998**, *167*, 109–118. [[CrossRef](#)]
7. Tesfahunegn, Y.A.; Rosa, F.; Gorla, C. The effects of the shape of tooth profile modifications on the transmission error, bending, and contact stress of spur gears. *Proc. Inst. Mech. Eng. Part C J. Mech. Eng. Sci.* **2010**, *224*, 1749–1758. [[CrossRef](#)]
8. Li, S.; Kahraman, A. A scuffing model for spur gear contacts. *Mech. Mach. Theory* **2021**, *156*, 104161. [[CrossRef](#)]

9. Hou, G.; Zhang, Y.; He, W.; Sun, X. Study on Influence of Profile Modification on Transmission Performance of Spur Gear. *IOP Conf. Ser. Mater. Sci. Eng.* **2018**, *389*, 012010. [[CrossRef](#)]
10. Imrek, H.; Düzcükoğlu, H. Relation between wear and tooth width modification in spur gears. *Wear* **2007**, *262*, 390–394. [[CrossRef](#)]
11. Choy, F.K.; Polyshchuk, V.; Zakrajsek, J.J.; Handschuh, R.; Townsend, D. Analysis of the effects of surface pitting and wear on the vibration of a gear transmission system. *Tribol. Int.* **1996**, *29*, 77–83. [[CrossRef](#)]
12. Mackaldener, M.; Flodin, A.; Andersson, S. Robust noise characteristics of gears due to their applications, manufacturing errors and wear. In *JSME International Conference on Motion and Power Transmission*; MPT: Fukuoka, Japan, 2001.
13. Zhang, J.; Liu, X. Effects of misalignment on surface wear of spur gears. *Proc. Inst. Mech. Eng. Part J J. Eng. Tribol.* **2015**, *229*, 1145–1158. [[CrossRef](#)]
14. Kumar, P.; Hirani, H.; Kumar Agrawal, A. Effect of gear misalignment on contact area: Theoretical and experimental studies. *Measurement* **2019**, *132*, 359–368. [[CrossRef](#)]
15. Alfares, M.A.; Falah, A.H.; Elkholy, A.H. Clearance distribution of misaligned gear coupling teeth considering crowning and geometry variations. *Mech. Mach. Theory* **2006**, *41*, 1258–1272. [[CrossRef](#)]
16. Tran, V.-T.; Hsu, R.-H.; Tsay, C.-B. Tooth contact analysis of double-crowned involute helical pairs shaved by a crowning mechanism with parallel shaving cutters. *Mech. Mach. Theory* **2014**, *79*, 198–216. [[CrossRef](#)]
17. Peng, Y.; Zhao, N.; Zhang, M.; Li, W.; Zhou, R. Non-Newtonian thermal elastohydrodynamic simulation of helical gears considering modification and misalignment. *Tribol. Int.* **2018**, *124*, 46–60. [[CrossRef](#)]
18. Beisekenov, I.; Spitas, C.; Amani, A.; Tsolakis, E.; Spitas, V. Stress analysis of self-aligning automotive gearing. *Int. J. Powertrains* **2019**, *8*, 93–114. [[CrossRef](#)]
19. Galym, Z.; Spitas, C. Analysis of a misalignment-insensitive spur gear transmission using a Rzeppa joint. *Proc. Inst. Mech. Eng. Part C J. Mech. Eng. Sci.* **2021**, *235*, 1670–1683. [[CrossRef](#)]
20. Temirkhan, M.; Tariq, H.B.; Kaloudis, K.; Kalligeros, C.; Spitas, V.; Spitas, C. Parametric Quasi-Static Study of the Effect of Misalignments on the Path of Contact, Transmission Error, and Contact Pressure of Crowned Spur and Helical Gear Teeth Using a Novel Rapidly Convergent Method. *Appl. Sci.* **2022**, *12*, 10067. [[CrossRef](#)]
21. Wang, S.; Zhu, R. An improved mesh stiffness model of helical gear pair considering axial mesh force and friction force influenced by surface roughness under EHL condition. *Appl. Math. Model.* **2022**, *102*, 453–471. [[CrossRef](#)]
22. Temirkhan, M.; Amrin, A.; Spitas, V.; Spitas, C. Convergence and accuracy problems of the conventional TCA model—Critical analysis and novel solution for crowned spur gears. *Proc. Inst. Mech. Eng. Part C J. Mech. Eng. Sci.* **2023**. [[CrossRef](#)]
23. Anand, A.; Irfan Ul Haq, M.; Vohra, K.; Raina, A.; Wani, M.F. Role of Green Tribology in Sustainability of Mechanical Systems: A State of the Art Survey. *Mater. Today Proc.* **2017**, *4*, 3659–3665. [[CrossRef](#)]
24. Ciulli, E. Tribology and Sustainable Development Goals. In *International Workshop IFToMM for Sustainable Development Goals, Proceedings of the I4SDG Workshop 2021, Online, 25–26 November 2021*; Quaglia, G., Gasparetto, A., Petuya, V., Carbone, G., Eds.; I4SDG 2021; Mechanisms and Machine Science; Springer: Cham, Switzerland, 2022; Volume 108. [[CrossRef](#)]
25. Elisaus, V.; Mohammadpour, M.; Theodossiades, S.; Rahnejat, H. Effect of teeth micro-geometrical form modification on contact kinematics and efficiency of high performance transmissions. *Proc. Inst. Mech. Eng. Part K J. Multi-Body Dyn.* **2017**, *231*, 146441931771015. [[CrossRef](#)]
26. Saketharaman, K.; Meenakshi, C.M.; Ravi, D. Analyzing the Life Prediction of Spur Gear based on Vinyl Ester with Different Fibre. *J. Phys. Conf. Ser.* **2022**, *2272*, 012014. [[CrossRef](#)]
27. Gohar, R.; Rahnejat, H. *Fundamentals of Tribology*, 2nd ed.; Imperial College Press: London, UK, 2012.
28. Johnson, K.; Tevarwerk, J. Shear Behaviour of EHL Oil Film. *Proc. R. Soc. A* **1977**, *356*, 215–236.
29. Roelands, C. Correlational Aspects of the Viscosity-Temperature-Pressure Relationships of Lubricating Oils. Ph.D. Thesis, Technical University Delft, Delft, The Netherlands, 1966.
30. Lugt, P.M.; Morales-Espejel, G.E. A Review of Elasto-Hydrodynamic Lubrication Theory. *Tribol. Trans.* **2011**, *54*, 470–496. [[CrossRef](#)]
31. Dowson, D.; Higginson, G. *Elastohydrodynamic Lubrication*; Pergamon: Oxford, UK, 1966.
32. Johnson, K. *Contact Mechanics*; Cambridge University Press: Cambridge, UK, 1985.
33. Al Tubi, I. Effects of Variable Load and Rotational Speed Conditions on Gear Micropitting in Wind Turbine Gearboxes. Ph.D. Thesis, University of Sheffield, Sheffield, UK, 2014.

Disclaimer/Publisher’s Note: The statements, opinions and data contained in all publications are solely those of the individual author(s) and contributor(s) and not of MDPI and/or the editor(s). MDPI and/or the editor(s) disclaim responsibility for any injury to people or property resulting from any ideas, methods, instructions or products referred to in the content.